THE DYNAMICAL EVOLUTION OF A TUBULAR LEONID PERSISTENT TRAIN

PETER JENNISKENS AND DAVID NUGENT
SETI Institute, NASA Ames Research Center, Mail Stop 239-4, Moffett Field, CA 94035
E-mail: pjenniskens@mail.arc.nasa.gov

and

JOHN M.C. PLANE
School of Environmental Sciences, University of East Anglia, Norwich NR4 7TJ, UK
E-mail: J.Plane@uea.ac.uk

(Received 26 May 2000; Accepted 16 August 2000)

Abstract. The dynamical evolution of the persistent train of a bright Leonid meteor was examined for evidence of the source of the luminosity and the physical conditions in the meteor path. The train consisted of two parallel somewhat diffuse luminous tracks, interpreted as the walls of a tube. A general lack of wind shear along the trail allowed these structures to remain intact for nearly 200 s, from which it was possible to determine that the tubular structure expanded at a near constant 10.5 ms^{-1}, independent of altitude between 86 and 97 km. An initial fast decrease of train intensity below 90 km was followed by an increase in intensity and then a gradual decrease at longer times, whereas at high altitudes the integrated intensity was nearly constant with time. These results are compared to a model that describes the dynamical evolution of the train by diffusion, following an initial rapid expansion of the hot gaseous trail behind the meteoroid. The train luminosity is produced by O (^1S) emission at 557 nm, driven by elevated atomic O levels produced by the meteor impact, as well as chemiluminescent reactions of the ablated metals Na and Fe with O_3. Ozone is rapidly removed within the train, both by thermal decomposition and catalytic destruction by the metallic species. Hence, the brightest emission occurs at the edge of the train between outwardly diffusing metallic species and inwardly diffusing O_3. Although the model is able to account plausibly for a number of characteristic features of the train evolution, significant discrepancies remain that cannot easily be resolved.

Keywords: Airglow, chemistry, dynamics, Leonids 1998, lower thermosphere, mesosphere, meteor, persistent train

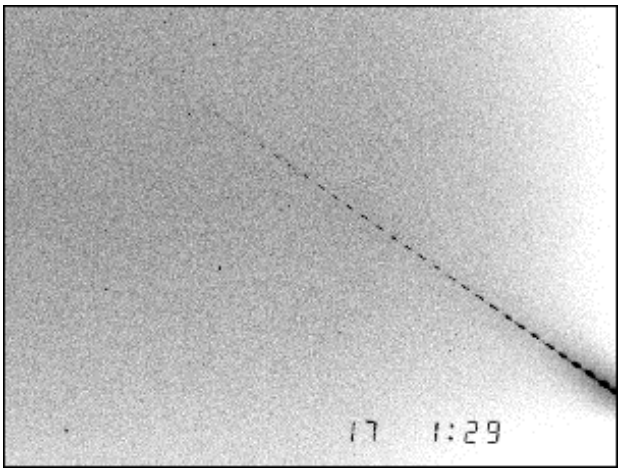

Figure 1. The 01:31:16 fireball photographed by Steve Evans of the British Astronomical Association – Meteor Section.

1. Introduction

Bright Leonid meteors are known for a characteristic long-lasting persistent glow that is called a *persistent train*. The luminous source of persistent trains has not been established, although it is generally believed that the reaction between ozone and atomic oxygen, efficiently catalysed by meteoric metals in the train itself, is the dominant mechanism (Kolb and Elgin, 1976; Poole, 1979; Baggaley, 1980; Hapgood, 1980).

Persistent trains probe upper atmosphere chemistry. Moreover, they enable probes of meteoric aerothermochemistry by providing direction to telescopes many minutes after the meteor has disappeared (Jenniskens *et al.*, 1998). Several such experiments during the Leonid Multi-Instrument Aircraft Campaign (Jenniskens and Butow, 1999a) have provided the first visual, near-IR and mid-IR spectroscopy of trains. In order to better interpret this spectroscopic information, we study here a rather striking example of a persistent train observed over the United Kingdom in 1998, in order to examine the evolution of trail width and intensity with time. Unlike many other trains, this train exhibited little distortion from wind shear along the trajectory and remained fairly linear during the observation period.

2. Observations

At 01:31:16 UT on November 17, 1998, a bright Leonid meteor (Figure 1) erupted over the southern U.K., moving from Southend-on-Sea to just beyond Reading. Amateur astronomer Sandy Osborough, from Chippenham, Wiltshire (51°28'N, 02°07'W), was located near the end point of the trajectory. The meteor was outside the field of view of his intensified video camera, but the scattered light in the atmosphere left a flash in the video record. Osborough adjusted the viewing direction of the camera and obtained a particularly nice record of the "Chippenham" persistent train between 15 seconds and 2m54s after the flash (Figure 2, right part of each frame). The train persisted longer than that, but the camera was pointed elsewhere. He used a 45 lp/mm ITT Night Vision gogles attached to a 3CCD Panasonic digital video camera. The close range of the train (116–80 km) produced a spatial resolution of 0.2 km/pixel.

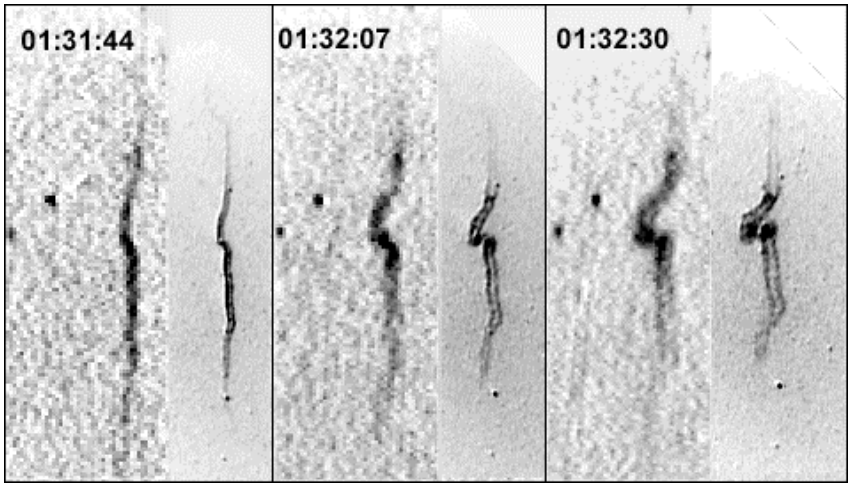

Figure 2. The train as seen by Tim Haymes from the perspective of Knowl Hill (left) and by Sandy Osborough from Chippenham (right).

The train was also filmed by Tim Haymes from Knowl Hill, Berks. (00°48' 51.3" W, 51° 30' 22.1" N), again from relatively short range (~102 km). Haymes used a 28 mm f/2 lens imaging onto an 18 mm 2nd generation MCP image intensifier (30 lpi). The image resolution was also 0.2 km/pixel, but the noisier tube created a less exceptional image.

From his perspective, the train was less foreshortened (Figure 2, left panels). Haymes also captured the diffuse beginning of the meteor, first detected at about 183 km altitude at 01:31:13 UT, until it left the field of view at 145 km. A bright flash was timed at 01:31:16 UT. After that, the camera was hand held and pointed at the train from 01:31:30 until 01:32:33 UT, and again from 01:34:58 until 01:35:17 UT when only the bright loop in the center of the train was visible as a diffuse blob. A faint sonic boom was heard around 01:36:40 UT, consistent with the distance from the meteor train. This is the second sonic boom reported for a bright Leonid fireball (ReVelle and Whitaker, 1999). Unfortunately, the convergence angle between the planes emanating from the two observing sites is only Q = 3°, too small for stereoscopic measurements.

Fortunately, the meteor was photographed by Steve Evans from Thurlow, near Newmarket in Suffolk (52° 7' 58".1 N, 0° 26' 49".1 E, Alt: 83m), in a 5m59s exposure on Ektapress 1600 commencing at 01:29:00 UT (Figure 1). The perspective was good, with a convergence angle Q = 29.8° with Chippenham and Q = 27.1° with Knowl Hill. Triangulation shows that the meteor entered the atmosphere at an angle of 29° with the horizon and came from an eastern azimuth of 87° from North from a direction Right Ascension 150.0 ± 0.3, Decl. 23.8 ± 0.3. The meteor was first detected at an altitude of 116 km and left the photograph at 86 km. The two linear parts of the train span the range 98 until 85 km, while the end point of the Chippenham train is at about 80 km altitude. Photometry of the meteor and stars gave a peak brightness of $M_v = -9 \pm 1$ magn. at the edge of the photograph. Beginning height and end height suggest a peak brightness of –10 ± 1 magn. in comparison to the trajectories calculated for other bright Leonid fireballs (Spurny *et al.*, 2000). The mass of the meteoroid was about 0.1 kg, within a factor of two.

3. Results

3.1. TRAIN MORPHOLOGY

The train consists of two parallel somewhat diffuse luminous trails, which are visible along the full length of the recorded trajectory. The double structure has been noted previously and is a characteristic feature of long lasting persistent trains (Jenniskens *et al.*, 1998). The diffuse trails show some amount of puffy billowing, which implies some amount of turbulence.

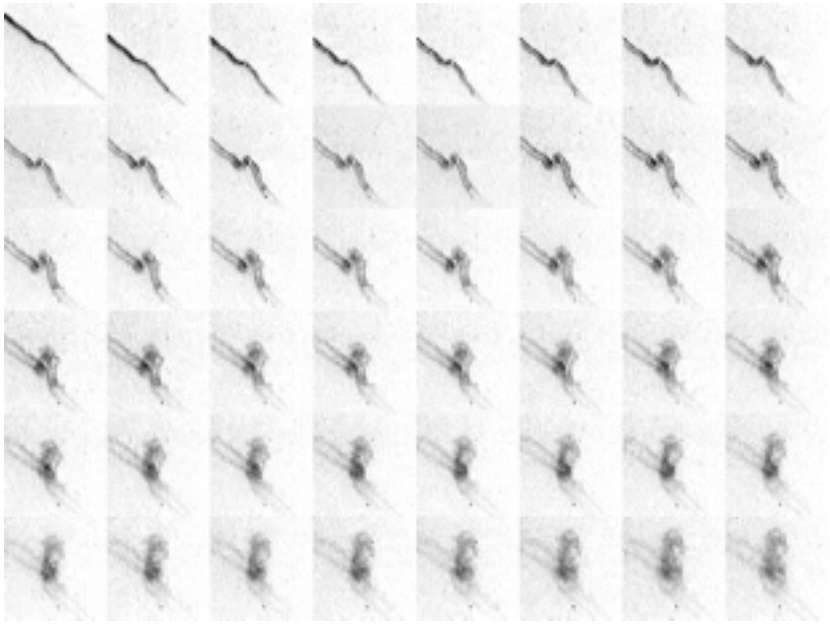

Figure 3. Sequence of images as seen from Chippenham between 0m15s and 02m52s after the meteor, showing the formation of the loop and the evolution of the linear parts.

This train is very unusual because the two straight sections of the trajectory remain almost straight with respect to the star background (Figure 3). Note that the lower part gradually gains upon the higher part and may be rising in altitude. Only the bright middle section forms a loop, which eventually overlaps in the line of sight. At the position of the loop, the wind direction changes dramatically with altitude. It is from the North in the straight sections, while from the East in the distorted middle part and end sections, with strong wind shears in the transition regions. The magnitude of the wind vector changes only by a factor of 2–3. Most of the wind shear is laminar, preserving the tubular structure of the train during distortion.

The morphology of the train is either that of a tube, where the two trails represent the longest line of sight along the walls of the tube, or they represent the turbulent top and bottom of a ribbon-like structure. The most likely morphology is that of a tube, for two reasons. First of all, from the somewhat different perspective of Knowl Hill, the train diameter (in km) is the same as that measured from Chippenham (Figure

2). Secondly, one can see that the distance between the two walls does not change where the train distorts in a knot and the line of sight cuts at a different angle through the train (Figure 3).

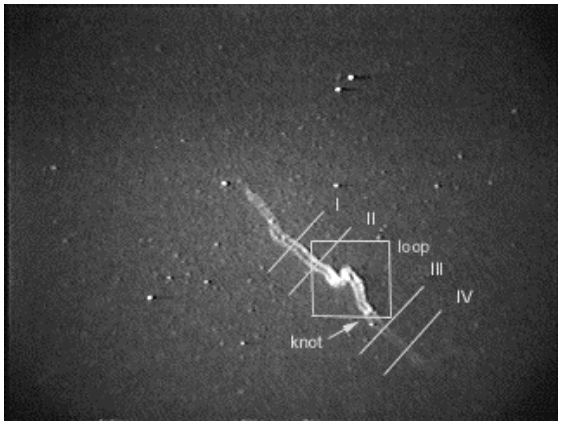

Figure 4. Full frame of the persistent train as seen from Chippenham at a time 45 seconds after the fireball. Four positions are indicated that were studied in detail, at altitudes 86 (I), 89 (II), 95 (III), and 97 (IV) km.

3.2. DYNAMIC EVOLUTION

Over time, one can see the walls of the tube separate and slightly thicken. We analyzed this behavior by fitting a set of two Gaussian curves to the variation of intensity in a slice perpendicular to the train at four positions indicated in Figure 4. The positions I–IV correspond to altitudes of about 86, 89, 95, and 97 km, respectively.

Figure 5a (top) shows the separation (in km) as a function of time. We find a constant expansion velocity of 10.5 ± 0.5 ms^{-1} for all positions. There is no sign of a slowing down over this time interval, except perhaps for the highest position at 97 km. The fact that the expansion is practically altitude independent between 85 and 98 km is surprising. In addition, the least-squares fit through the data does not extrapolate to zero separation at zero time, but yields a positive intercept of 0.13 ± 0.03 km. This may signify an initial rapid expansion of the train, but the small value does not exclude a more mundane artifact of the measurement procedure.

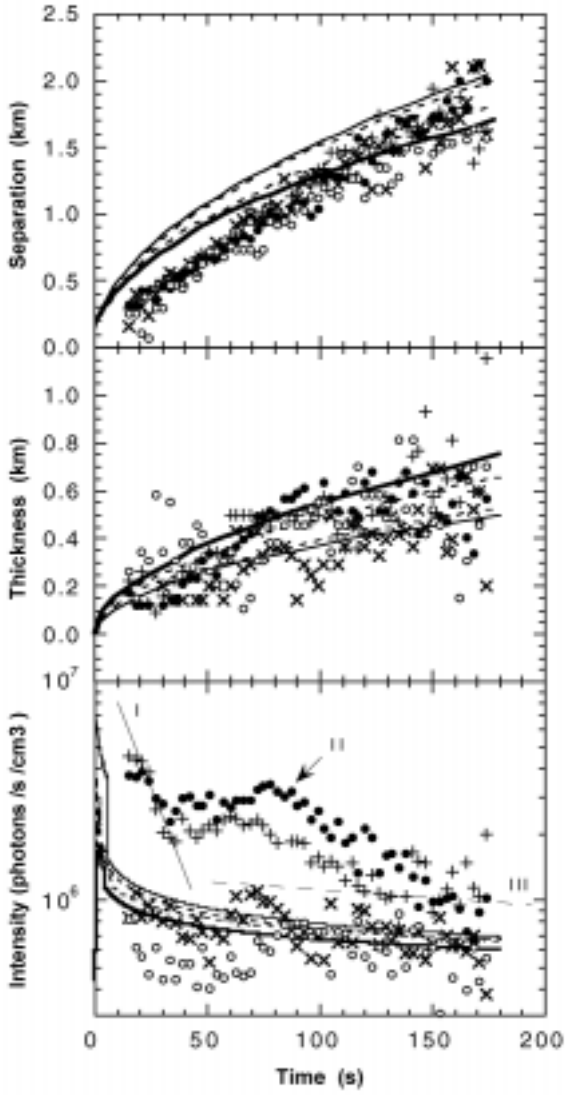

Figure 5. (a) The separation between the peak intensity of the tubular walls; (b) the thickness of the tubular wall; and (c) the integrated intensity of the tubular walls as a function of time. Symbols are: Pos. I (•), Pos. II (+), Pos. III (x), Pos. IV (o). Model results shown are for 86 (solid line), 89 (dashed), 95 (dashed) and 97 km altitude (thick solid line).

The tubular walls are resolved at the end of the exposure. We measured the thickness at half peak intensity as a function of time and deconvolved with a 2-pixel wide Gaussian response curve. We find that the turbulent walls tend to show slightly more billowing over time, gradually thickening, but the expansion slows down after about 100 s (Figure 5b).

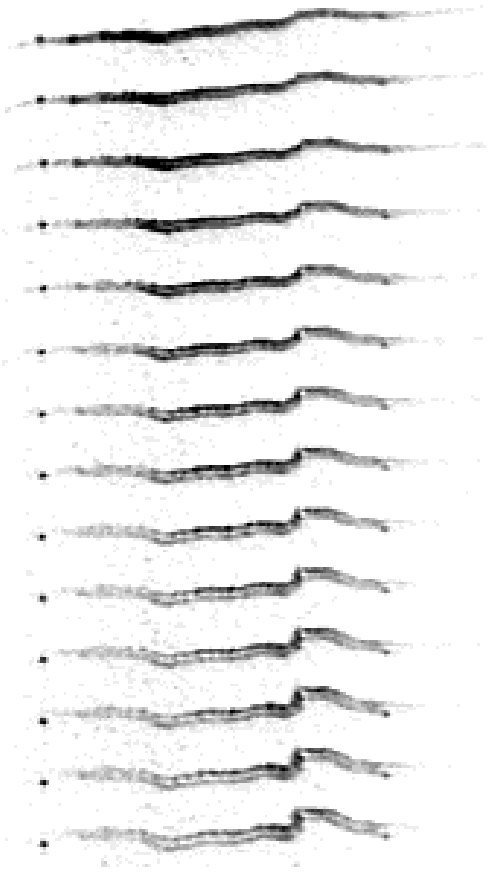

Figure 6. Altitude dependent decay of emission during the first period from 15.0 to 34.5 seconds after the meteor (in intervals of 1.5 seconds). A star (left) is shown for brightness reference.

The two sides of the tube do not have the same intensity at positions I and II (Figure 6). One side is brighter by up to 50% over the other. The integrated intensity of both tubular walls shows three distinct periods of decay, particularly below 90 km (Figure 5c, bottom graph). An initial fast decay (I) is followed by an increase in intensity, which after some time decreases again (II). At the end of the observing time the train decay rate slows significantly (III).

Phase (I) has a decay time of about 15 seconds, which is slightly altitude dependent. This altitude dependence is apparent when viewing the train intensity in the meteor video during the first 30 seconds (Figure

6). The brightness decays fastest at the lower altitude end of the train (left in Figure 6), while the higher altitudes follow in succession.

Phase (II) is characterized by the initial brightening of the train. The intensity peaks earliest towards the middle part of the trajectory, with mechanisms delaying the increase at very high and very low altitudes. The subsequent decay has a time constant of about 63 ± 2 s at 86 km, 70 ± 2 s at 89 km, 150 ± 20 s at 95 km, and about 190 s at 97 km altitude.

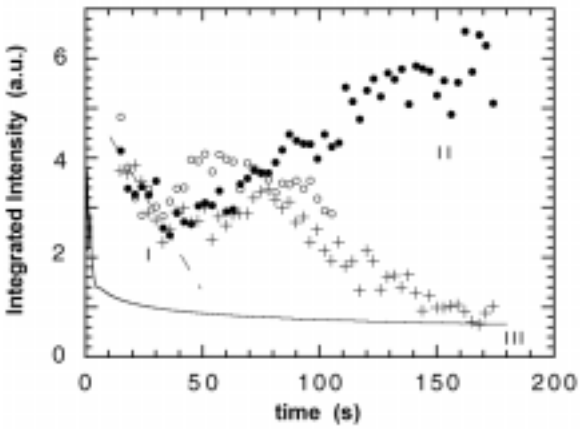

Figure 7. Integrated intensity variation of the knot (•) and the total intensity of the loop (o), scaled to that of the "quiet" train at position I (+). Solid line shows a model fit for the height of 86 km (in units of 10^6 photons cm^{-3} s^{-1}).

This intensity increase during Phase (II) may be related to the brightening phenomenon that enhances the brightness of the loop between 90 and 94 km. The integrated intensity of the loop (box in Figure 4) is shown in Figure 7, in relation to the brightness of the linear part of the train at position II. At the end of the observation, the loop is the only part that remains clearly visible. A remarkable feature is the "knot" (marked in Figure 4), where wind shear appears to be particularly high at the beginning of the observations. We see that the tubular structure breaks down during bending and a wall of billowing emission is observed. Here, we find the quickest brightness increase, which is followed by a decrease that mimics the linear part of the train (open circles in Figure 7).

Phase (III) is most apparent in the high altitude part of the train, but also visible in position II. This phase represents the late stages of train evolution. It is well represented by our model calculations below.

4. Discussion

4.1. A MODEL OF A PERSISTENT METEOR TRAIN

The persistent train luminosity is thought to be caused by the catalytic recombination of ozone and oxygen atoms by meteoric metal atoms (Chapman, 1956; Kolb and Elgin, 1976; Poole, 1979; Baggaley, 1980). Recent spectroscopic observations of persistent trains during the Leonid MAC mission and at the Weybourne Atmospheric Observatory in Norfolk (Jenniskens *et al.*, 2000b) have confirmed that the most intense emission arises from the Na D-line, almost certainly through the Chapman airglow mechanism:

$$Na + O_3 \rightarrow NaO + O_2 \quad (1)$$

$$NaO + O \rightarrow Na(3^2P, 3^2S) + O_2 \quad (2)$$

where the branching ratio of reaction 2 to produce the Na (3^2P) state (which then emits an orange photon at 589 nm) is about 10% (Clemesha *et al.*, 1995). Molecular emission bands also probably arise from:

$$Fe + O_3 \rightarrow FeO(^5\Delta \text{ etc.}) + O_2 \quad (3)$$
$$FeO + O \rightarrow Fe + O_2 \quad (4)$$

where reaction 3 is sufficiently exothermic to produce FeO in excited electronic states, leading to emission in the “orange arc” bands between 570 and 630 nm with about a 2 % efficiency (Helmer and Plane, 1994). Other metals such as Ca and K will also contribute to the overall emission intensity, but the ablated concentrations of these metals are much lower (Plane, 1991).

If we now assume that the twin tracks of the observed train are due to a luminous tube with a dark center when viewed from below (e.g. Figure 8), then the explanation for the dark center must be that O_3, which “fuels” these chemiluminescent reactions, has been consumed. The same hypothesis was made independently in a recent paper by Kelley *et al.* (2000). Of course, these emissions also depend on atomic O to complete the catalytic cycles. However, O is in excess over O_3 by about 3 orders of magnitude in the ambient nighttime upper mesosphere, and the meteoric impact on the atmosphere causes the dissociation of O_2 to

produce additional O (the green tail of Leonid meteors, in particular, is caused by emission from O (^{1}S) which is highly dependent on the atomic O concentration, as discussed below). The depletion of O_3 could arise both from thermal dissociation in the initially very hot train, and metal-catalysed destruction. Effective catalytic removal places a lower limit on the concentration of metallic species produced by ablation. Note that all neutral metal atoms, as well as metallic ions with the exception of the alkali metal ions, participate in catalytic O_3 destruction (Plane and Helmer, 1994).

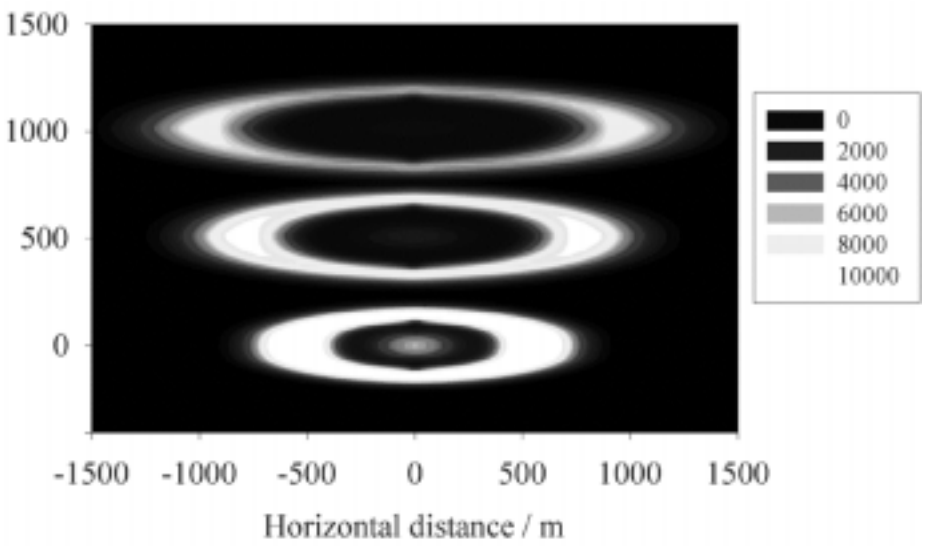

Figure 8. Three cross-sections through the persistent train at an altitude of 86 km, showing the modeled emission intensity at times 50s (bottom), 100s and 150s after the meteor. The 100 and 150 s sections have been displaced upward by 500 and 1000 m, respectively, for the purpose of presentation. The central emission patch visible at 50 s and 100 s is due to [OI] emission, the outer ring is due to chemiluminescence from metal atom reactions with ambient ozone.

We have therefore constructed a model of a Leonid meteor train in order to simulate the train expansion, the increase in wall thickness and the observed brightness variation as a function of position and time. The model makes the following assumptions:

1. The meteoroid ablates according to the deceleration equation (particle density = 3,200 kg m^{-3}, drag coefficient = 0.75 and shape factor = 1.2 for a sphere) and heat transfer equation (heat of sublimation = 2 x 10^6 J kg^{-1} and heat transfer coefficient = 0.5) given

by Hughes (1992). Fragmentation is not considered in this simple model. In order to provide sufficient metallic species to cause effectively total removal of O_3.in the centre of the train after 50 s, the initial meteoroid mass has to be in excess of 0.1 kg. The simulations shown here employed an initial mass of 0.2 kg, at the upper end of the estimated mass of the Chippenham meteoroid (see above).

2. Even at the very low pressures of the upper mesosphere/lower thermosphere ($< 10^{-5}$ bar), the size and velocity of this meteoroid would create a turbulent wake (Reynolds number > 2,000). Thus we assume that the train radius is initially 30 m, in which the air is then heated almost instantaneously to 2,100 K. The resulting pressure increase by more than a factor of 10 creates a shock wave which expands radially. Assuming that this expansion occurs adiabatically, then the pressure will equilibrate with the background atmosphere when the radius is about 70 m, leaving a train temperature of about 1,100 K. This train radius and temperature are predicted to be nearly constant between 97 and 86 km (heights IV and I in Figure 4), with the concentration of ablated metallic species ranging from 2.5×10^9 to 9.9×10^9 cm^{-3} at these respective heights. The ambient O_3 within this initial train volume would be thermally decomposed.
3. Following this very rapid expansion on a time-scale of less than a second (the speed of sound is 270 ms^{-1} in this region), the subsequent expansion of the train is controlled by the diffusion of mass and heat. For the modelling exercise presented here, this was allowed to vary as a function of height and be different in the horizontal and vertical, with the lower limit being the atomic diffusion coefficient of Na (Helmer and Plane, 1993).
4. The reaction rate coefficients for 1–4 were taken from Plane and Helmer (1994). The relative concentrations of Na and Fe were assumed to be in their meteoritic ratio, about 1:8 (Plane, 1991).
5. On the relatively short time scale of the train (minutes rather than hours), and particularly in the presence of elevated concentrations of atomic O, it is very unlikely that the metallic species would be able to form more stable reservoir compounds such as $NaHCO_3$ or $Fe(OH)_2$. Indeed, between 85 and 100 km in the background atmosphere the meteoric metals are overwhelmingly in the atomic form (Plane *et al.*, 1999).
6. The "green line" emission at 557 nm from the O ($^1S - {}^1D$) transition (termed [OI]) was assumed to be produced by the Barth mechanism with the absolute intensity calculated using the parameterisation of

Murtagh *et al.* (1990). Assuming that this emission dominates the train emission immediately after the meteor, then in order to simulate the observed decrease in intensity of the Chippenham train at longer times the model requires that about 15% of the O_2 in the initial train was dissociated.

The train model was then run with a spatial resolution of 25 meter and integration time-step of 0.2 seconds. Figure 8 shows cross sections through the modelled train at an altitude of 86 km at 50s, 100s and 150s after the meteor. Initially, strong [OI] emission is observed at the center of the trail because of the enhanced O atom concentration produced from dissocation of atmospheric O_2 by the meteor. The [OI] intensity is dependent on $[O]^3$, so that the intensity falls very quickly as the atomic O diffuses outwards from the centre of the train.

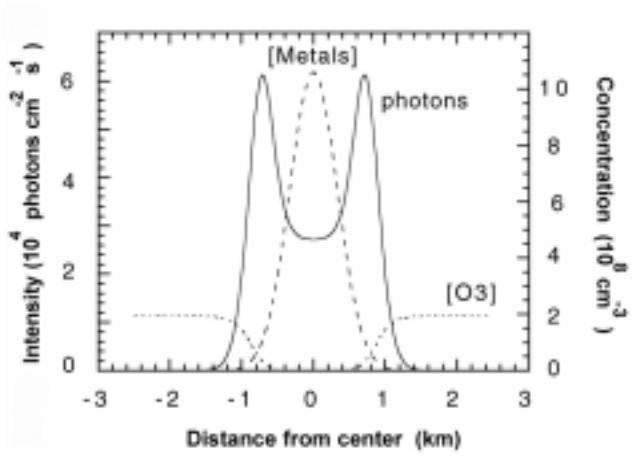

Figure 9. Variation in the metal atom and O_3 densities across the center of the trail at 98 km, 100 s after the meteor. The vertically integrated emission intensity which would be observed from the ground, is shown for comparison.

As shown in Figure 9, after 100 s the O_3 concentration within the train has been reduced by orders of magnitude by the combined effects of thermal decomposition and catalytic destruction. The concentration profile of the metallic species is approximately Gaussian, as expected for diffusion-controlled transport. The metallic emission is strongest at the edge of the train, where fresh ambient O_3 is diffusing inwards.

For reasonable diffusion rates, the model does account for the general widening of the train, the tubular structure, and the increase of the train width. The model also explains phase III in the brightness decay.

The model simulations of the wall separation, the wall thickness, and the integrated intensity are plotted as a function of time in Figure 5 for comparison with the observations at positions I–IV. In the case of the wall separation (Figure 5a), the model is able to simulate the "average" observed rate of separation over the first 180 s by using a horizontal diffusion coefficient ranging from (5–7) x 10^6 cm^2 s^{-1} between 86 and 97 km, and a vertical diffusion coefficient set to the larger of either the vertical eddy diffusion coefficient K_{zz} employed in 2D atmospheric models [Garcia and Solomon 1994], or the molecular diffusion coefficient with a temperature $T^{1.8}$ dependence (Helmer and Plane, 1993). The reason for choosing different horizontal and vertical coefficients is discussed below.

Inspection of Figure 5a shows that the model, being based on diffusive transport necessarily produces a separation that varies as time $t^{1/2}$, whereas the observed separation increases linearly with time at all four heights. This striking observation remains unexplained. Free expansion is ruled out, because the passing meteor cannot have affected the air density over such large volume. Interestingly, the thickness of the walls does increase much more like $t^{1/2}$ (Figure 5b), in accord with a diffusion-controlled process. Note that the rapid initial expansion of the train to a wall separation of about 150 m, driven by a shock-heated pressure wave (see above), is in good accord with the extrapolated intercepts of the observed separations at the four heights (Figure 5a).

Although there is reasonable overall agreement, the model is unable to match the contrast between the dark center and the walls that is apparent in the images. Figure 10 illustrates the vertically integrated emission intensity across the train when viewed from below, comparing model and observation at 89 km, 160 s after the meteor. If the trail is indeed a cylinder with a luminous wall and dark center, then the model predicts that the contrast between the center and the brightest part of the walls, as seen from the ground, is about 0.5, remaining roughly constant with time. This factor arises simply from the fact that when viewed from the ground, the center is seen against the top and bottom of the cylinder and therefore cannot be very dark. By contrast, we observe an exponential decrease of contrast to about 0.1 after 120 s. The symbols in Figure 10 show the train cross-section between 153 s and 165s at positions I and III. The data have been scaled to the model curve to compare the contrast

between the central minimum and the wall maxima. In fact, the lack of contrast in the model is all the more striking because we have maximised the contrast by using a smaller vertical diffusion coefficient to reduce the vertical transport of metallic species and fresh O_3, thereby minimising the wall brightness in the top and bottom parts of the tube (Figure 8). The lack of contrast is not explained by decreasing the initial ozone concentration in the center faster, for example as a result of photodissociation of ozone by the meteoric UV light (Zinn *et al.*, 1999).

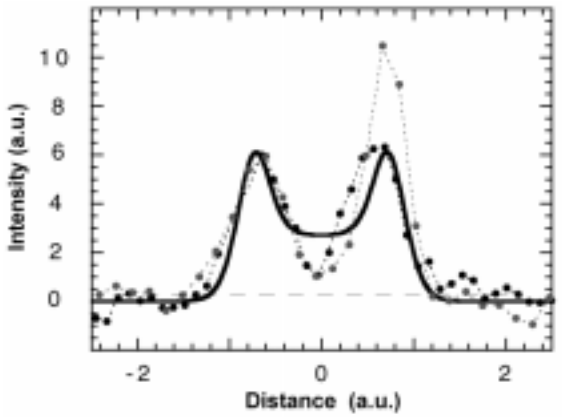

Figure 10. Contrast in brightness of center and walls in model (solid line) and observations. Model in units of 10^4 photons cm^{-3} s^{-1}.

Also, there are significant difficulties with modeling the brightness behavior (Figure 5c). The phase I decay is thought to be due to emission of the forbidden 557 nm O ($^1S - {}^1D$) transition. Indeed, meteors of lesser brightness are known to have persistent emission on a time scale of about 10 seconds, sometimes referred to as the meteor "wake" (Halliday, 1958). This is a direct result of molecular oxygen dissociation by the meteor and has been well recorded in photographic and TV video spectra (e.g. Borovicka *et al.*, 1996). Figure 11 reproduces one of our own measurements, where it can be seen that the [OI] emission starts shortly after the meteor itself, peaks, and then rapidly decays. The model predicts that the [OI] emission in the Chippenham train would have been brighter at and below 90 km (positions I and II), since this is where more atomic O is produced in the meteor. The emission is predicted to decay on a time scale of only about 10 s (due to its $[O]^3$ dependence and the rapid outward diffusion of atomic O), rather than the observed 30 - 40 s

in phase I. Note also that the [OI] line intensity should be concentrated in the center of the train (Figure 8), rather than the train walls, whereas from Figure 6 it is clear that at least part of the early decay is the result of emission from the train walls.

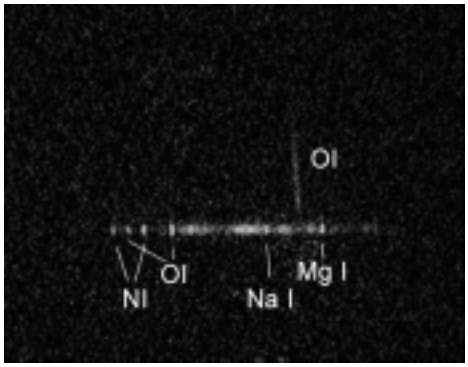

Figure 11. Forbidden line emission of OI in the wake of a –1 Leonid meteor (Nov. 17, 1998, 19:31:11 UT). This first order spectrum was taken with a low-resolution visible spectrometer onboard FISTA during the 1998 Leonid MAC (Jenniskens and Butow, 1999). The meteor moved from top to bottom. Short wavelengths are to the right.

The models predict very little change in intensity over the 174 s of observations that comprise Phase II in Figure 5c. This is because as the peak intensity of the walls decreases so the thickness of the walls increases with time, and hence the integrated intensity hardly changes. This behavior does reproduce the phase III behavior as signified by the decay of intensity observed at altitudes above 90 km, and also correctly predicts that the intensity at lower altitudes of 86 and 89 km will eventually decrease to similar levels. However, the complex time evolution of the intensity at these lower altitudes, particularly the intensity increase of Phase II, remains unexplained

4.2. ALTERNATIVE TRAIN MODELS

The present model does not include a detailed treatment of small-scale turbulent mixing at the boundary of train and ambient air. The observations seem to suggest that wind shear enhances the observed luminosity, and the walls show clear signs of billowing. This could

increase the interfacial area between the train and surrounding air, enhancing the rate of chemiluminescent reactions between metallic species and O_3. If such turbulence spread horizontally rather than vertically, this would help to explain the high contrast between train center and walls.

The model assumes that the longer-lived emission is due to metallic atoms reacting with O_3. A rapid decline in train intensity, such as observed in phase II at 86 and 89 km, could be because of depletion of these metals. However, there are no reactions with background atmospheric constituents such as H_2O, CO_2, O_2 etc. that will convert these species to stable forms on the time scale observed. The only other possibility is that these metals are reacting with the high concentration of silicates and other debris in the trail, although again the time scale of 200 seconds is very short.

In summary, the present model coupling meteor ablation with simple diffusive transport of the resulting train is able to account satisfactorily for some of the significant features of this unusual event. These include the appearance of two luminous tracks, the average rate of increase of their separation and thickness, and some aspects of the luminous emission decay. However, the model fails to explain the strikingly constant rate of separation increase, which cannot be diffusive in nature, and the complex variation of the emission with time at some altitudes, amongst others. Clearly, there is still much to be understood about the nature of persistent trains.

Acknowledgments

Amateur observers Sandy Osborough, Tim Hayes and Steve Evans are congratulated with their fine records of train and meteor. We are thankful for their kindness in making these records available for analysis. We also thank John Green and David Stephens at the University of East Anglia for helpful discussions on turbulent transport. This work forwards the goals of the Pro-Amat working group of IAU Commission 22. The work is supported by grants from NASA's Suborbital MITM and Exobiology programs, and by the NASA Advanced Missions and Technology program for Astrobiology. *Editorial handling:* Noah Brosch.

References

Baggaley, W.J.: 1980, in Halliday, I., and McIntosh, B.A., (eds.), *Solid Particles in the Solar System*. IAU Symp. 90, pp. 85–100.

Borovicka, J., Zimnikoval, P., Skvarka, J., Rajchl, J., and Spurny, P.: 1996, Astron. Astrophys. **306**, 995–998.

Borovicka, J., Stork, R., and Bocek, J.: 1999, *Meteoritics Planet. Sci*. **34**, 987–994.

Chapman, S.: 1956, in A. Dalgorno, E.B. Armstrong (eds), *The Airglow and the Aurorae*., Permagon Press, New York, pp. 204-.205.

Clemesha, B.R., Simonich, D.M. Takahashi, H. Melo, S.M.L, and Plane, J.M.C.: 1995, *J. Geophys. Res.* **100**, 18909–18916.

Garcia, R.R., and Solomon, S.: 1994, *J. Geophys. Res.* **99**, 12937–12951.

Halliday, I.: 1958, *Astrophys. J.* **128**, 441–443.

Hapgood, M.A.: 1980, *Nature* **286**, 582–583.

Helmer, M., and Plane, J.M.C.: 1993, *J. Geophysical Res.* **98**, 23207–23222.

Helmer, M., and Plane, J.M.C.: 1994, *Journal of the Chemical Society, Faraday Transactions* **90**, 31–37.

Hughes, D.W.: 1992, *Space Science Reviews* **61**, 275–299.

Jenniskens, P.: 1998, *Meteoritics Planet. Sci.* **33**, 955–957.

Jenniskens, P., de Lignie, M., Betlem, H., Borovicka, J., Laux, C.O., Packan, D., and Kruger, C.H.: 1998, Earth, *Moon and Planets* **80**, 311–341.

Jenniskens P., and Butow S.J., 1999, *Meteoritics Planet. Sci.* **34**, 933–943.

Jenniskens P., Butow, S.J., and Fonda, M.: 2000, *Earth, Moon and Planets* **82–83**, 1–26.

Jenniskens, P., Lacey, M., Allan, B.J., Self, D.E., and Plane, J.M.C.: 2000b, *Earth, Moon and Planets* **82–83**, 433–442.

Kelley, M.C., Gardner, C., Drummond, J., Armstrong, W.T., Liu, A., Chu, X., Papen, G., Kruschwitz, C., Loughmiller, P., and Engleman, J.: 2000, *Geophys. Res. Lett.* **27**, 1811–1814.

Kolb, C. E., and Elgin, J. R. (1976), *Nature* **263**, 488–490.

Murtagh, D.P., Witt, Stegman, J., McDade, I.C., Llewwellyn, E.J., Harris, F., and Greer, R.G.H.: 1990, *Planetary and Space Science* **38**, 43–53.

Plane, J.M.C.: 1991, *International Reviews of Physical Chemistry* **10**, 55–106.

Plane, J.M.C., and Helmer M.: 1994, In: *Research in Chemical Kinetics*, G. Hancock and R.G. Compton, eds, Elsevier, Amsterdam, 313–367.

Plane, J.M.C., Cox, R.M., and Rollason, R.J.: 1999, *Advances in Space Research* **24**, 1559–1570.

Poole, L.M.G.: 1979, *J. of Atmosph. Terr. Phys.* **41**, 53–64.

ReVelle, R.O., and Whitaker, R.W.: 1999, *Meteoritics Planet. Sci.* **34**, 995–1005.

Spurny, P., Betlem, H., Van 't Leven, J., and Jenniskens, P.: 2000, *Meteoritics Planet. Sci.* **35**, 243–249.

Zinn, J., Wren, J., Whitaker, R., Szymanski, J., ReVelle, D.O., Priedhorsky, W., Hills, J., Gisler, G., Fletcher, S., Casperson, D., Bloch, J., Balsano, R., Armstrong, W.T., Akerlof, C., Kehoe, R., McKay, T., Lee, B., Kelley, M.C., Spalding, R.E., and Marshall, S.: 2000, *Meteoritics Planet. Sci* **34**, 1007–1015.